JOURNAL OF VIROLOGY, Nov. 1997, p. 8632–8641 Vol. 71, No. 11
0022-538X/97/$04.00+0

Immunopathologic Changes in the Thymus during the Acute Stage of Experimentally Induced Feline Immunodeficiency Virus Infection in Juvenile Cats

JENNIFER C. WOO,[1] GREGG A. DEAN,[2] NIELS C. PEDERSEN,[2] AND PETER F. MOORE[1]*

Departments of Pathology, Microbiology, and Immunology[1] and Medicine and Epidemiology,[2] School of Veterinary Medicine, University of California, Davis, California 95616

Received 2 April 1997/Accepted 4 August 1997

The feline thymus is a target organ and site of viral replication during the acute stage of feline immunodeficiency virus (FIV) infection. This was demonstrated by histologic, immunohistologic, flow cytometric, and virologic tests. Thymic lesions developed after 28 days postinoculation (p.i.) and included thymitis, premature cortical involution, and medullary B-cell hyperplasia with germinal center formation and epithelial distortion. Alterations in thymocyte subsets also developed. Fewer $CD4^+$ $CD8^-$ cells were detected at 28 days p.i., while an increase in $CD4^-$ $CD8^+$ cells resulted in an inversion of the thymic CD4/CD8 ratio of single-positive cells, similar to events in peripheral blood. Provirus was present in all thymocyte subpopulations including cortical $CD1^{hi}$, $CD1^{lo}$, and B cells. The $CD1^{hi}$ thymocyte proviral burden increased markedly after 56 days p.i., coincident with the presence of infiltrating inflammatory cells. Increased levels of provirus in the $CD1^{lo}$ thymocyte subpopulation were detected prior to 56 days p.i. This was likely due to inclusion of infected infiltrating inflammatory cells which could not be differentiated from mature, medullary thymocytes. Proviral levels in B cells also increased from 70 days p.i. Morphologic alterations, productive viral infection, and altered thymocyte subpopulations suggest that thymic function is compromised, thus contributing to the inability of FIV-infected cats to replenish the peripheral T-cell pool.

Human immunodeficiency virus type 1 (HIV-1) infection is characterized by progressive depletion and qualitative dysfunction of peripheral CD4 T cells (27). In adult HIV-1 infection, thymic infection resulting in loss of residual thymic function may explain the lack of restoration or dysfunction of peripheral CD4 T cells, despite antiretroviral therapy (27). HIV-1 infection of the thymus is also believed to play a major role in the immunopathogenesis of pediatric AIDS. Involvement of the thymus in pediatric HIV-1 infection is suggested by rapid progression (12), abnormal peripheral T-lymphocyte subset development (16), and pronounced thymic lesions. Thymic lesions described for pediatric AIDS patients include severe thymic involution, HIV-1 infection of thymocytes, and selective depletion of $CD4^+$ $CD8^+$ and $CD4^+$ $CD8^-$ thymocytes (22, 26).

Although thymic involvement is thought to play an important role in pediatric AIDS, it has been difficult to prospectively or sequentially study thymic lesions in infants and children due to ethical and logistic limitations. Furthermore, thymic lesions in macaques experimentally infected with simian immunodeficiency virus (SIV) are not consistently reported during the acute stage of infection (13, 14, 18–20), although severe thymic involution (13, 19) is seen in the later stages of infection. The development of B-cell follicles as a component of the thymic lesion also occurs in both HIV-1 (3) and SIV (15) infection, although the presence of other viral infections in SIV has made these lesions difficult to interpret. However, documented similarities in clinical syndrome and pathogenesis between HIV-1 and acute feline immunodeficiency virus (FIV) infection (1, 2, 10, 11, 23) suggest that FIV may be an appropriate model of disease. FIV infection of juvenile cats was therefore employed in this study to further examine lentivirus-induced thymic dysfunction.

We have previously reported thymic lesions in juvenile cats experimentally infected with FIV (2). However, this time course study was undertaken to investigate the pathogenesis of these lesions. In addition, viral thymocyte targets were determined and thymus function was indirectly assessed by examination of thymocyte subpopulations in conjunction with peripheral blood T-cell events. Our findings indicate that the thymus is a site of viral replication in acute FIV infection. Severe structural and inflammatory changes and altered thymocyte subsets suggest that FIV infection reduced the ability of the thymus to replenish the peripheral T-cell pool. This likely contributed to peripheral T-cell lymphocytopenia. The thymus therefore plays a crucial role in the immunopathogenesis of FIV, particularly in juvenile cats.

MATERIALS AND METHODS

Experimental design. Specific-pathogen-free cats at 3 to 4 months of age were obtained from the breeding colony of the Feline Nutrition Laboratory, University of California, Davis. Sixteen cats were inoculated with FIV by intraperitoneal injection with 1 ml of whole heparinized blood from cat 5000 (chronically infected with the FIV-Petaluma biologic isolate) as described elsewhere (10). Two FIV-infected cats were killed at each of the following time points: 14, 28, 42, 56, 70, 84, 96, and 140 days postinfection. Age-matched control cats were killed at days 0, 56, 70, 84, and 140 of the study. This design therefore mapped development of the thymic lesion from the acute phase (weeks 0 to 15) to the early asymptomatic stage (weeks 16 to 20) of FIV infection. Age-matched control animals were required to account for age-related thymic involution, which commences around 6 to 8 months of age.

Animals and tissues. Peripheral blood was collected from each animal into tubes containing EDTA as an anticoagulant every second week and prior to euthanasia. Complete blood counts and leukocyte differential counts were performed by standard techniques (1). Peripheral blood CD4 and CD8 T-lymphocyte counts were performed on each blood sample by flow cytometry as described elsewhere (8). Virus isolation from plasma was performed by coculture of plasma with uninfected cat peripheral blood mononuclear cells as described previously (25). Culture supernatants were tested for FIV core protein by enzyme-linked immunosorbent assay as described previously (7). Serum antibodies to FIV were

* Corresponding author. Mailing address: Department of Pathology, Microbiology, and Immunology, School of Veterinary Medicine, University of California, Davis, Davis, CA 95616. Phone: (916) 752-6611. Fax: (916) 752-3349. E-mail: pfmoore@ucdavis.edu.

TABLE 1. MAbs which recognize feline leukocyte antigens

Antigen	MAb	Features
CD1	Fe1.5F4 (IgG1)	49-kDa β2 microglobulin-associated molecule expressed by cortical thymocytes and medullary dendritic antigen-presenting cells
CD4	Fe1.7B12 (IgG1)	60-kDa glycoprotein expressed by immature cortical thymocytes, a subpopulation of mature medullary thymocytes, and a helper-inducer T-cell subpopulation in peripheral blood
CD8	Fe1.10E9 (IgG1)	28- to 32-kDa heterodimer expressed by immature cortical thymocytes, a subpopulation of mature medullary thymocytes, and a cytotoxic-suppressor T-cell subpopulation in peripheral blood
CD21	Fe2.8F9 (IgG1)	145- to 160-kDa antigen expressed by a B-lymphocyte subpopulation in peripheral blood, B cells in lymphoid follicles, and germinal center follicular dendritic cells in peripheral tissues
CD22	Fe2.9F2 (IgG1)	135-kDa antigen expressed by a B-lymphocyte subpopulation in peripheral blood and B cells within lymphoid follicles in peripheral lymphoid tissues
Cytokeratins 8, 18, and 19	5D3 (IgG1) (BioGenex)	Stains cortical thymocyte epithelial network but has reduced expression on medullary thymocyte epithelium

detected by enzyme-linked immunosorbent assay as previously described (10). After sedation with ketamine HCl (Boehringer Ingelheim Corp., St. Joseph, Mo.), cats were killed by intracardiac injection of 10 ml of saturated KCl solution. At necropsy, the thymus was weighed and measured. Pieces of thymic tissue (3 to 5 mm) were either fixed in 10% buffered formalin prior to paraffin embedding for routine histopathology or embedded in OCT compound (Tissue-Tek; Sakura Finetek USA, Torrance, Calif.) before snap freezing in liquid N_2-cooled isopentane (Fisher Scientific, Pittsburgh, Pa.). The remaining fresh tissue was minced to generate a single-cell suspension of thymocytes. Cells were washed in RPMI 1640 (Mediatech; Fisher Scientific) with 10% horse serum and 0.1% sodium azide and filtered twice through cotton gauze to remove connective tissue and cell debris. Thymocyte aggregation was inhibited by adding 100 U of DNase I (Calbiochem, San Diego, Calif.) per 5×10^7 thymocytes.

Monoclonal antibodies (MAbs) and reagents. A panel of MAbs specific for feline leukocyte antigens (Table 1) was used to label cells for immunohistology, immunofluorescence, flow cytometric analysis, and paramagnetic bead enrichment of thymocyte subpopulations. A cytokeratin MAb (5D3; BioGenex, San Ramon, Calif.), specific for cytokeratins 8, 18, and 19, was used to examine the thymic epithelium. Antibodies were generally used as tissue culture fluid (TCF) at a 1:10 dilution for tissue staining and used undiluted for flow cytometry and magnetic bead enrichment. Antibody conjugates were generated for multiple-label immunofluorescence and flow cytometry experiments as described previously (30). The CD4 MAb (Fe1.7B12) was fluorescein isothiocyanate (FITC) conjugated, the CD8 MAb (Fe1.10E9) was R-phycoerythrin (RPE) conjugated, and CD1 (Fe1.5F4) and CD22 (Fe2.9F2) MAbs were biotinylated. Biotinylation of the CD1 MAb permitted the use of the tandem dye streptavidin-RPE-CY5 (Southern Biotechnology, Birmingham, Ala.) in conjunction with the other two fluorochromes for triple-label flow cytometry. The same biotinylated reagents were also utilized for dual-label immunofluorescence in addition to the biotin-conjugated CD4 MAb (Fe1.7B12). Custom conjugation of 1 mg of CD1-specific immunoglobulin G1 (IgG1) to paramagnetic microbeads (Miltenyi Biotec, Auburn, Calif.) enabled magnetic bead enrichment of cortical $CD1^{hi}$ thymocytes. Goat anti-mouse IgG microbeads (Miltenyi Biotec) were also used in conjunction with CD21- and CD22-specific TCF for enrichment of B cells from the thymocyte pool.

Immunohistology. Frozen OCT-embedded thymus tissues were sectioned, and 6-μm thin sections were collected onto poly-L-lysine (Sigma Chemical Co., St. Louis, Mo.)-coated slides. Sections were stained by the avidin-biotin-peroxidase complex technique or by indirect immunofluorescence as previously described (17). Undiluted TCF of the appropriate antibody was applied to sections of thymus. An irrelevant mouse myeloma (IgG1) served as a negative control. Double-label immunofluorescence was performed by incubating thymic tissues with TCF specific for CD1, CD8, or cytokeratin followed by horse anti-mouse IgG Texas red (Vector Laboratories, Burlingame, Calif.). An intermediate blocking step with an irrelevant mouse IgG1 ascitic fluid was performed before a second incubation with a biotinylated antibody specific for either CD4, CD8, or CD22 followed by goat antibiotin FITC-conjugated antibody (Vector Laboratories). A dual-channel immunofluorescent filter system (Chroma, Brattleboro, Vt.; part no. 51006) permitted viewing of Texas red and FITC emission signals simultaneously.

Flow cytometry. Thymocytes were labeled with MAb TCF followed by horse anti-mouse FITC-conjugated antibody (Vector Laboratories) as described previously (17). An irrelevant mouse myeloma (IgG1) TCF served as a negative control. For double- and triple-label experiments, similar cell preparations were incubated with titered amounts of directly conjugated antibodies (CD4-FITC, CD8-RPE, and CD1-biotin). For three-color experiments, the biotin-stained cell preparations were subsequently incubated with the tandem dye streptavidin-RPE/CY5. Stained cells were analyzed with a FACScan analytical cytometer (Becton Dickinson, San Jose, Calif.) equipped with Lysis II software (Becton Dickinson).

Magnetic bead enrichment. Enrichment of immature $CD1^{hi}$ thymocytes was achieved by using CD1 custom-conjugated paramagnetic microbeads (Miltenyi Biotec) as per the manufacturer's recommendation. After incubation with 25 μl of conjugated microbeads, 5×10^7 thymocytes were passed through a 30-μm-pore-size preseparation filter (Miltenyi Biotec) and an MS MACS separation column (Miltenyi Biotec) attached to a MiniMACS magnet (Miltenyi Biotec). Cells retained by the column ($CD1^{hi}$) were eluted. Cells which passed through the column ($CD1^{lo}$) were subjected to further enrichment for CD21 and CD22 cells. The unretarded fraction ($CD1^{lo}$) was subsequently incubated with a combination of 100 μl each of CD21- and CD22-specific TCF for 15 min. After washing, cells were incubated with 100 μl of goat anti-mouse IgG1 microbeads (Miltenyi Biotec) before being passed a second time through a preseparation filter and an MS MACS separation column. Cells which passed through the column were mature thymocytes with a single-positive CD4 or CD8 phenotype ($CD1^{lo}$). Cells retained by the column were B cells. All fractions, including $CD1^{hi}$, $CD1^{lo}$, and B-cell fractions, were analyzed for the degree of enrichment by flow cytometry. The degree of enrichment was calculated for $CD1^{hi}$ fractions as a percentage of cells within the population with high-density CD1 antigen expression. The percent purity of the $CD1^{lo}$ fraction was calculated as a percentage of cells within the population with intermediate to low expression of CD1.

Nucleic acid isolation. Nucleic acid was isolated from pieces of thymus and enriched $CD1^{hi}$, $CD1^{lo}$, and B-cell thymocyte subpopulations. A single-cell suspension from thymus was generated with a Cellector (Bellco Glass Inc., Vineland, N.J.). Cells from either whole thymus or paramagnetic-bead-enriched thymocyte subpopulations were pelleted by centrifugation at $1,000 \times g$, resuspended in Tri reagent (5×10^6 cells/ml) (Molecular Research Center, Cincinnati, Ohio), and stored at −70°C prior to DNA and RNA extraction. Samples were processed to extract DNA and RNA as per the manufacturer's directions with minor modifications. Briefly, 0.2 volume of chloroform was added to the cell pellet before centrifugation at $12,000 \times g$ to obtain a phase separation. After collection of the aqueous and organic phases, 0.5 volume of isopropanol and 0.05 volume of RNA Tack resin (Biotecx, Houston, Tex.) were added to the aqueous phase containing the RNA. The resin-bound RNA was pelleted and washed twice with 70% ethanol. RNA was subsequently eluted in 0.1 volume of diethyl pyrocarbonate-treated water. Samples were incubated with 40 U of RNase-free DNase (Boehringer Mannheim, Indianapolis, Ind.) and 20 U of RNasin (Promega Inc., Madison, Wis.) at 37°C for 60 min and then at 95°C for 5 min. The RNA concentration was determined spectrophotometrically (A_{260}) (Genquant II; Pharmacia, Uppsala, Sweden). DNA was precipitated from the organic phase by adding 0.3 volume of 100% ethanol. After sedimentation by centrifugation at $2,000 \times g$, the DNA pellet was washed twice with 75% ethanol, dried under vacuum, and then dissolved in 8 mM NaOH. The DNA concentration was also determined spectrophotometrically (A_{260}).

Nested FIV-*gag* PCR. Seminested PCR of proviral DNA was performed as previously described (23). PCR was performed on 1 μg of DNA with primers specific for the FIV *gag* gene sequence (primers NP37 and NP38 in the first round and NP38 and NP39 in the second round) (24). Two PCR rounds were performed in a BioOven III thermal cycler (BioTherm Corp., Fairfax, Va.). Each round consisted of 35 cycles (30 s of template denaturation at 94°C, 30 s of primer annealing at 55°C, and 45 s of primer extension at 72°C). PCR products were analyzed by electrophoresis through a 2% agarose–1× Tris-acetate–EDTA electrophoresis buffer followed by ethidium bromide staining.

FIV RT-PCR. One microgram of RNA was reverse transcribed with a reverse transcription (RT) kit (Promega). An FIV-*gag*-specific primer (NP38) was used for RT. The reaction mixture was incubated for 60 min at 42°C followed by 5 min

at 95°C. Samples were subsequently subjected to PCR with seminested *gag* primers as described above. Parallel samples were processed without reverse transcriptase to ensure that contaminating proviral DNA was not present in the extracted RNA.

FIV quantitative competitive (QC)-PCR. A competitive template was generated with a PCR MIMIC construction kit (Clontech Laboratories, Inc., Palo Alto, Calif.). Primers NP37 and NP38 were added to the MIMIC to generate a 423-bp template product after PCR in comparison to a native 466-bp FIV proviral DNA product. A standard curve was generated by performing PCR on a series of samples containing 10-fold dilutions of native template (10^1 to 10^7 molecules) with a constant amount (10^4 molecules) of competitor (FIV-MIMIC) (31). The same number of molecules of FIV-MIMIC was also added to 1 μg of DNA isolated from thymus samples as described above. A single round of PCR consisting of 35 cycles (30 s of template denaturation at 96°C, 30 s of primer annealing at 55°C, and 45 s of primer extension at 72°C) was performed in a BioOven III thermal cycler. PCR products were analyzed by electrophoresis through 3% Metaphor agarose (FMC Bioproducts, Rockland, Maine)–1× Tris-acetate–EDTA electrophoresis buffer followed by ethidium bromide staining. Band intensities were determined with a Fotodyne Eclipse system with Collage software (Fotodyne Inc., Hartland, Wis.). A standard curve was generated by plotting the log ratio of native to MIMIC band intensities (abscissa) versus the log native molecule number (ordinate) of the standard curve samples (31). A linear regression provided a formula from which the number of FIV *gag* molecules in unknown samples was calculated. Samples used to generate the standard curve and unknown samples were always processed simultaneously such that each PCR series had its own standard curve.

Statistical analysis. Results from flow cytometric analyses of both peripheral blood CD4/CD8 T-cell ratio and thymocytes were subjected to regression analysis. For each time point, nonsimultaneous 95% confidence intervals were calculated. Significant differences between FIV-inoculated and noninfected control cats were declared where upper and lower confidence intervals of each group, respectively, for each time point, failed to overlap.

RESULTS

Peripheral hematologic changes. Hematologic changes, including lymphopenia and neutropenia, which developed from 42 days postinoculation (p.i.), were similar to those previously described (2, 10) and consistent with changes described for this Petaluma strain of FIV. The peripheral CD4/CD8 T-cell ratio decreased significantly ($P < 0.05$) from 42 days p.i. in FIV-infected cats and continued to decline throughout the study (Fig. 1A). This was associated with the decline in peripheral CD4 T cells (Fig. 1B), as peripheral CD8 T cells remained constant throughout the study (Fig. 1C). Virus was isolated from plasma from 14 days p.i. and was present thereafter throughout the study. Serum antibodies were detected in 15 of 16 FIV-inoculated animals by 14 days p.i. One cat (cat 94009) was excluded from the study due to its failure to seroconvert or to demonstrate viral infection of peripheral blood or thymic tissue.

Thymic morphology. Gross lesions of the thymus were not apparent. Thymic weight among noninfected control cats varied with age. In control cats, the highest weight was recorded at day 84. The decreased thymic weight in control cats recorded at day 140 was attributed to age-associated involution. By contrast, the thymic weight of FIV-infected cats remained low throughout the period of the study. Those thymuses examined at days 70 and 140 p.i. were markedly smaller than those of the age-matched control cats. Thymic weights for FIV-infected cats were highest at 84 to 96 days p.i., coinciding with the period of maximum B-cell infiltration (Fig. 2). An exception was observed in one animal (cat 5268) at 84 days p.i., at which B-cell infiltration and severe cortical involution occurred (Table 2).

Histologically, thymic lesions were initially detected in one of two cats killed at 28 days p.i. However, by 42 days p.i., FIV-infected animals consistently exhibited similar thymic lesions characterized by thymitis, cortical involution, and medullary lymphoid follicular hyperplasia with germinal center formation. Thymitis, manifested by interlobular infiltration of lymphocytes, was present at 28 days p.i. Thymitis and encroachment of infiltrating lymphocytes into the adjacent cortical tissue became increasingly evident from 56 days p.i. Marked cortical thymic involution, characterized by severe depletion of cortical thymocytes, was also increasingly evident beyond 56 days p.i. Cortical involution occurred in an irregular pattern and, in association with encroachment of lymphocytes into the cortex, resulted in an increasingly poor distinction between cortical and medullary zones in the thymus beyond 70 days p.i. (Fig. 3A and B). An almost complete disappearance of cortical thymocytes was observed beyond 96 days p.i. Medul-

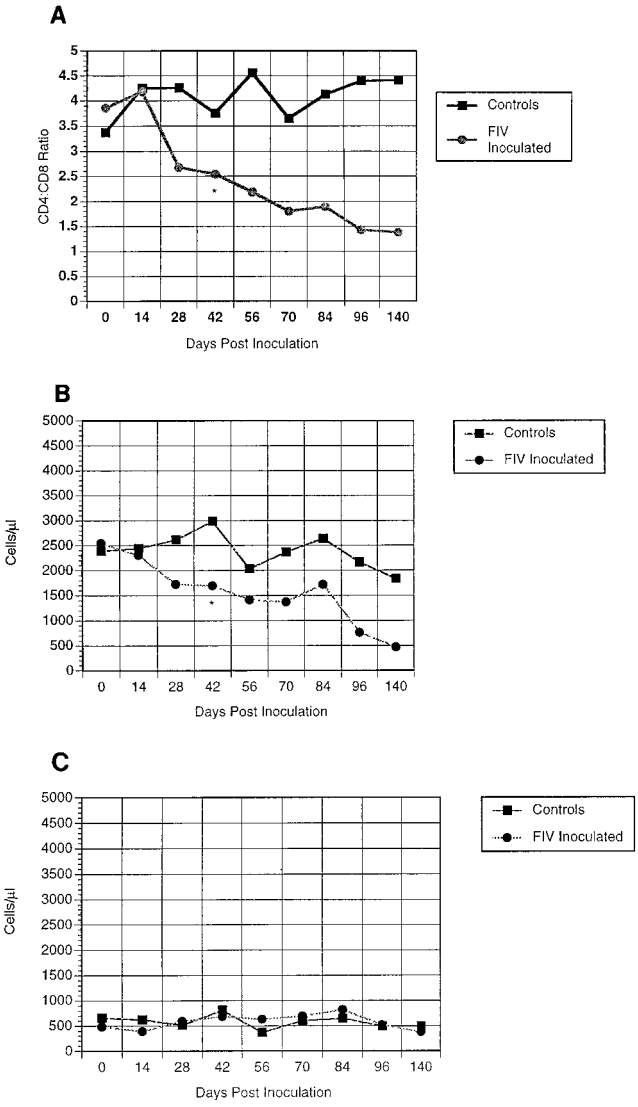

FIG. 1. Time course of peripheral blood lymphocyte events in FIV-infected and noninfected control cats. (Each point represents the mean value of all surviving animals at that time point and includes those killed at that time point according to the schedule described for the experimental design.) (A) Peripheral CD4/CD8 T-cell ratio in FIV-infected and noninfected control cats. A significant decrease in CD4/CD8 T-cell ratio was detected from 42 days p.i. in FIV-infected cats (*, $P < 0.05$). (B) Absolute values of peripheral CD4 T lymphocytes in FIV-infected cats demonstrate a decline in peripheral CD4 T cells during the course of infection relative to noninfected control cats. A significant decrease in peripheral CD4 T cells was detected from 42 days p.i. in FIV-infected cats. (*, $P < 0.05$). (C) Absolute values of peripheral CD8 T lymphocytes in FIV-infected cats and noninfected control cats demonstrate little variation in CD8 T cells during the course of infection. Significant differences between the FIV-infected and noninfected groups were not detected.

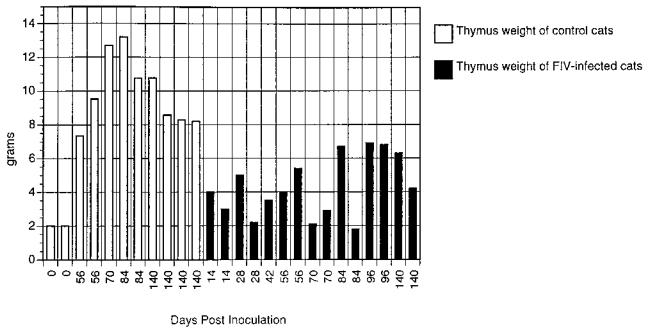

FIG. 2. Thymus weights from FIV-infected and noninfected control cats. Thymic atrophy manifested by low thymic weight is consistently present in FIV-infected cats. (Each bar represents the thymus weight of each animal.)

lary lymphoid follicular hyperplasia developed from 56 days p.i. Prior to 56 days p.i., lymphoid follicle formation was characterized by small focal aggregates of lymphocytes within the medulla and adjacent corticomedullary junction. These follicles increased in size from 56 to 84 days p.i. Follicular enlargement during this period was accompanied by germinal center formation. During the later stages of the experimental period (96 to 140 days p.i.), the thymus exhibited multiple highly misshapen lymphoid follicles which were distinguished from the thymic parenchyma by an irregular mantle of lymphocytes (Fig. 3C).

Leukocyte antigen expression in the thymus. The integrity of the thymic cortex was further evaluated by immunohistologic examination of CD1, CD4, and CD8 antigen expression. CD1 expression in noninfected control cats was limited to cortical thymocytes and medullary dendritic antigen-presenting cells (Fig. 4A). Both CD4 and CD8 expression was present on cortical thymocytes in high density, consistent with cortical, dual-positive ($CD4^+$ $CD8^+$) expression. Medullary thymocyte expression of CD4 and CD8 antigens was relatively sparse, compatible with single-positive ($CD4^+$ $CD8^-$ or $CD4^-$ $CD8^+$) expression on medullary thymocyte subpopulations (Fig. 4C and D). Flow cytometric analysis demonstrated a continuum of expression of CD1, CD4, and CD8 antigens on thymocytes, ranging from low to intermediate to high density. Age-associated thymic involution in noninfected control cats was characterized by a decline in high-density CD1 expression and an increase in intermediate- to low-density CD1 expression. A similar age-associated decrease in thymocyte CD4 and CD8 expression occurred.

In the FIV-infected thymus, minimal change was detected prior to 28 days p.i. by immunohistology. Sequential examination of thymic tissue at subsequent time points demonstrated an irregular but progressive pattern of premature CD1 thymocyte loss which corresponded to areas of cortical involution seen histologically. By 96 days p.i., CD1 expression was confined to single occasional cells within the lobule. Immunohistologic observations were confirmed by flow cytometry (Table 2). Reduced numbers of CD1 thymocytes were detected in FIV-infected cats from 42 days p.i. (Table 2). A precipitous decrease in CD1 thymocytes occurred at 56 to 70 days p.i., and few CD1 thymocytes remained beyond 96 days p.i. Recovery of CD1 expression in FIV-infected animals was not detected during the time course of this study.

Sparse focal B-cell (CD21-CD22) infiltration of the thymic cortex of FIV-infected cats was observed from 28 days p.i. and coincided with the thymitis lesion observed histologically.

TABLE 2. Leukocyte antigen expression of the feline thymocyte population[a]

Cat no.[b]	Days p.i.	$CD1^+$	$CD4^+$ $CD8^+$	$CD4^+$ $CD8^-$	$CD4^-$ $CD8^+$	CD4/CD8 ratio	$CD21^+$	$CD22^+$
94005 C	0	82.66	60.84	16.37	12.28	1.33	<1	<1
95007 C	0	75.68	58.55	14.55	13.20	1.10	<1	<1
95399 C	56	82.99	58.94	11.50	10.74	1.07	<1	<1
95407 C	56	80.65	60.66	11.14	10.46	1.06	<1	<1
5274 C	70	70.44	64.13	15.48	9.48	1.63	<1	<1
95454 C	84	82.71	59.02	11.50	10.67	1.07	<1	<1
95477 C	84	81.99	61.78	12.14	10.34	1.17	<1	<1
5265 C	140	85.44	50.91	15.35	9.58	1.6	<1	<1
5270 C	140	59.92	51.79	14.05	11.76	1.19	<1	<1
95441 C	140	62.94	52.00	14.05	13.65	1.03	<1	<1
95449 C	140	70.76	55.09	13.36	11.81	1.13	<1	<1
94006	14	71.18	56.88	11.70	10.41	1.12	<1	<1
94010	14	79.04	69.21	12.00	8.53	1.40	<1	<1
94011	28	74.69	63.86	8.90*[c]	13.22	0.67*	<1	<1
94012	28	71.21	55.70	9.31	11.31	0.82	<1	<1
94008	42	59.22	56.34	10.70	23.94*	0.45	<1	<1
5263	56	43.30*	6.40*	5.53	28.03	0.14	22.58	24.96
5266	56	17.58	6.24	5.56	24.56	0.22	10.9	9.52
5264	70	10.36	11.96	6.57	22.78	0.28	24.14	24.96
5272	70	30.9	28.85	6.14	13.69	0.44	19.02	21.16
5267	84	22.04	12.87	7.81	14.06	0.55	65.06	55.94
5268	84	3.80	4.08	5.29	20.59	0.25	45.18	42.7
5262	96	4.90	1.04	6.68	15.15	0.44	49.82	51.58
5269	96	10.24	6.57	5.85	18.62	0.31	53.78	41.1
5271	140	6.20	6.13	10.65	13.14	0.81	30.7	37.55
5273	140	8.92	7.13	10.88	12.29	0.88	47.07	32.22

[a] Data are expressed as percentages of the thymocyte population.
[b] C, age-matched control cat.
[c] *, significant difference ($P < 0.05$) from noninfected control cats recorded at this and subsequent time points.

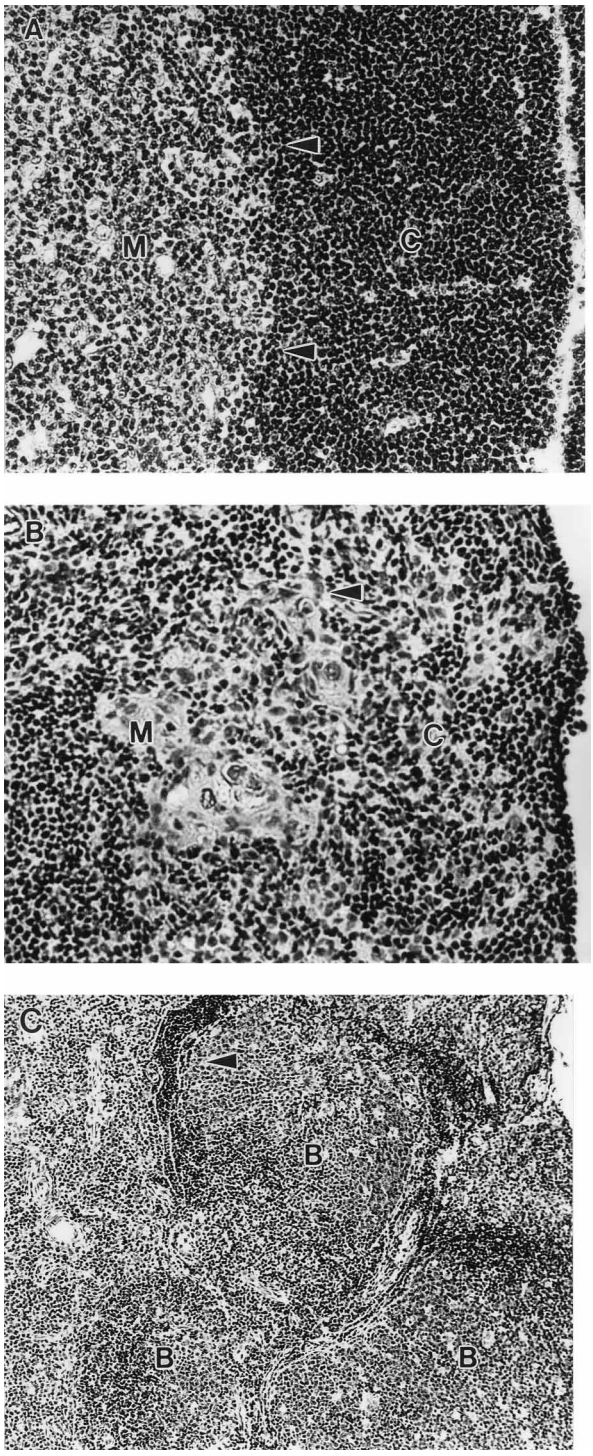

FIG. 3. Histologic lesions of the feline thymus after FIV infection (hematoxylin and eosin stain). (A) A distinctive corticomedullary junction (arrowheads) defines the cortex (C) from the medulla (M) in the thymus of an age-matched control cat at the day 70 time point. Magnification, ×140. (B) Cortical involution and loss of corticomedullary definition (arrowhead) result in poor distinction between cortex (C) and medulla (M) in the FIV-infected feline thymus at 56 days p.i. Magnification, ×140. (C) Multiple prominent B-cell follicles (B) with germinal center formation defined by a prominent marginal zone (arrowhead) were present at 140 days p.i. Magnification, ×70.

However, by flow cytometry, B cells constituted less than 1% of cells in the thymus of all noninfected control animals throughout the study and were not detected in FIV-infected cats until 56 days p.i. (Table 2). After 56 days p.i., B cells comprised an increasing percentage of the thymocyte pool (Table 2). Immunohistology correspondingly demonstrated focal infiltration of B cells in the cortex and corticomedullary junctions of thymic lobules. B-cell foci also corresponded to areas of lymphoid follicular hyperplasia. B-cell follicles were associated with an extensive follicular dendritic cell network as determined by CD21 staining. These foci frequently extended from the medullary region to the interlobular septa, resulting in an irregular dissection of B cells throughout the lobule. In contrast to the expected distribution of cytokeratin in the thymus (Fig. 4B), cytokeratin staining revealed considerable distortion and loss of the epithelial cytokeratin network, which correlated with the development of expansive B-cell follicles (Fig. 5B and E). By examining adjacent sections of thymus, the areas of thymitis and B-cell follicular development could be mapped to areas where loss of CD1 cortical thymocytes had occurred (Fig. 5A). Double immunofluorescent staining, which enabled examination of cytokeratin and CD22 expression simultaneously, demonstrated that the thymic epithelium and B cells were mutually exclusive populations (Fig. 6B).

Medullary B-cell follicles were infiltrated by CD4 and CD8 cells (Fig. 5C and D). This was increasingly evident after 56 days p.i. Double immunofluorescence demonstrated that CD4 and CD8 cells, within both the thymic medulla and B-cell follicles, were of single-positive phenotype (Fig. 6C). Although both CD4 and CD8 cells were observed within germinal centers, CD8 cells predominated within the thymic tissue. $CD4^-$ $CD8^+$ cells increased significantly ($P < 0.05$) from 42 days p.i. and comprised between 12 and 28% of the thymocyte pool compared to noninfected control cats, which averaged 11% $CD4^-$ $CD8^+$ cells throughout the study period (Table 2). By contrast, $CD4^+$ $CD8^-$ cells decreased significantly ($P < 0.05$) from 28 days p.i. and remained at reduced levels compared to noninfected control cats, which averaged 15% $CD4^+$ $CD8^-$ cells, throughout the study. This variation in CD4 and CD8 cells at each time point was assessed by using the ratio of single-positive CD4 to CD8 cells in the thymus (Table 2). In noninfected control cats, the thymic CD4/CD8 ratio averaged 1.37. This ratio was significantly decreased ($P < 0.05$) in all FIV-infected cats from 28 days p.i. This shift in thymocyte subsets developed prior to the period in which the peripheral blood CD4/CD8 T-cell ratio significantly decreased at 42 days p.i.

Sorted thymocyte subpopulations. Separation of $CD1^{hi}$ fractions in control animals with paramagnetic beads resulted in a purity of 95 to 99% for $CD1^{hi}$ fractions. In FIV-infected cats, 80 to 88% purity for $CD1^{hi}$ fractions and 88 to 98% purity for $CD1^{lo}$ fractions were achieved during the period from 14 to 42 days p.i. However, after 56 days p.i., separation of $CD1^{hi}$ fractions without contamination with $CD1^{lo}$ cells was not achieved due to the paucity of $CD1^{hi}$ cells in infected cats. Separation of B cells (CD21-CD22) from the thymocyte pool was not performed before 56 days p.i. due to the paucity of B cells at earlier time points. From 56 to 140 days p.i., B cells were sorted to 85 to 95% purity.

Proviral burden in sorted thymus subpopulations. Low levels of FIV provirus (<100 copies/μg of DNA) were detected in the enriched $CD1^{hi}$ thymocyte population at 28 and 42 days p.i. However, by 56 days p.i., the proviral burden in $CD1^{hi}$ cells was dramatically increased to greater than 10,000 proviral copies per μg of DNA as determined by QC-PCR. The proviral burden remained high (between 100 and 75,000 proviral copies/μg

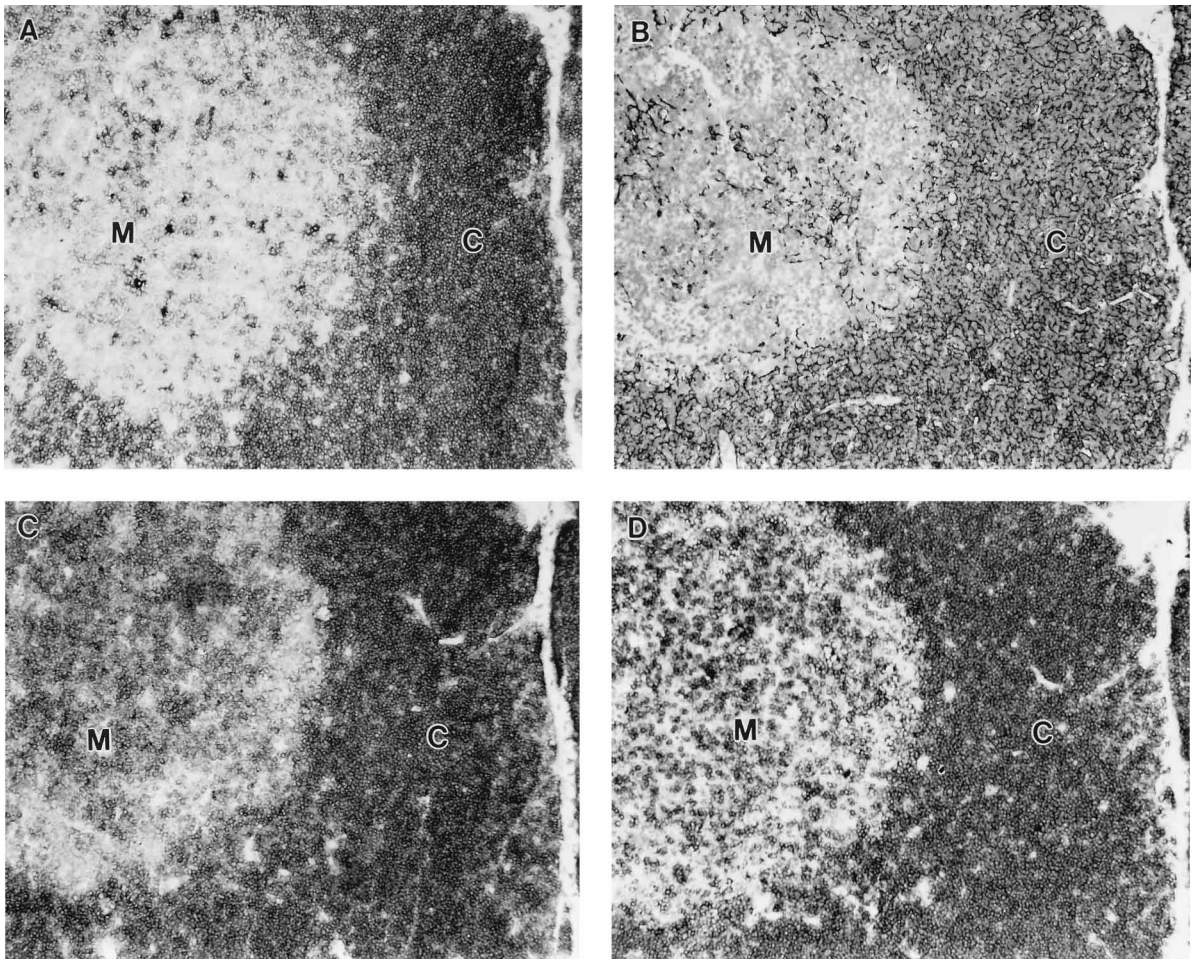

FIG. 4. Immunohistology of serial sections of the normal thymus of a noninfected control cat at 84 days of the study (immunoperoxidase and then hematoxylin counterstain). (A) CD1 MAb (Fe1.5F4) staining of a thymic lobule in a noninfected control cat at 84 days of the study demonstrates the expected CD1 expression, which is limited to cortical thymocytes (C) and sparser antigen-presenting cells in the thymic medulla (M). Magnification, ×70. (B) Cytokeratin MAb (5D3) staining demonstrates the arborizing cortical epithelial network (C). Reduced expression of this antibody on the medullary epithelium (M) facilitates immunohistologic distinction between cortical and medullary zones of the thymic lobule. Magnification, ×70. (C) CD4 MAb (Fe1.7B12) staining demonstrates the expected distribution of CD4, which is present in high density on cortical thymocytes (C), compatible with dual-positive $CD4^+$ $CD8^+$ thymocyte expression. CD4 expression is sparser on medullary thymocytes (M), compatible with single-positive $CD4^+$ $CD8^-$ expression. Magnification, ×70. (D) CD8 MAb (Fe1.10E9) staining demonstrates the expected distribution of CD8, which is present in high density on cortical thymocytes (C) but is sparser on medullary thymocytes (M), compatible with single-positive $CD4^-$ $CD8^+$ expression. Magnification, ×70.

of DNA) in the $CD1^{hi}$ population throughout the remainder of the experimental period (Fig. 7A). By contrast, the proviral burden in the $CD1^{lo}$ population was high (3,600 to 45,000 copies/μg of DNA) at 28 days p.i. and remained high throughout the sampling period (Fig. 7B). Provirus was detected in the enriched B-cell population from 56 days p.i. but was less than 10 copies/μg of DNA. However, by 70 days p.i., proviral levels in B cells were similar to that observed in the T-cell subsets. Exceptions were observed at 84 days p.i., when no proviral DNA was detected in B cells by seminested PCR in one animal, and at 140 days p.i., when less than 10 proviral copies/μg of DNA were measured in one of two animals tested (Fig. 7C).

RT-PCR for FIV RNA was also performed on enriched thymocyte subpopulations. Quantitation was not possible due to limited amounts of RNA available from sorted populations. Viral RNA was detected in the $CD1^{hi}$ population in all provirus-positive cats. Viral RNA was also detected in 12 of 13 cats and 8 of 9 cats for $CD1^{lo}$ thymocytes and B cells, respectively. No uninoculated control animals were positive for FIV provirus or RNA, and all sorted samples with undetectable provirus were also negative for viral RNA.

DISCUSSION

The progression of thymic lesions associated with acute FIV infection in juvenile cats was examined over a period of 140 days. We demonstrated that the thymus is a major target organ for viral infection and replication during the acute stage of infection. Severe structural lesions and thymocyte subset alterations indicated that FIV infection reduced the ability of the thymus to replenish the peripheral T-cell pool. This likely contributes to peripheral T-cell lymphocytopenia, which develops in FIV-infected cats.

Significant pathologic and immunopathologic changes, characterized by thymic atrophy and B-cell follicular hyperplasia, were demonstrated in young cats in the acute stage of experimental FIV infection. These changes appeared permanent, as there was no evidence of thymic regeneration during the sub-

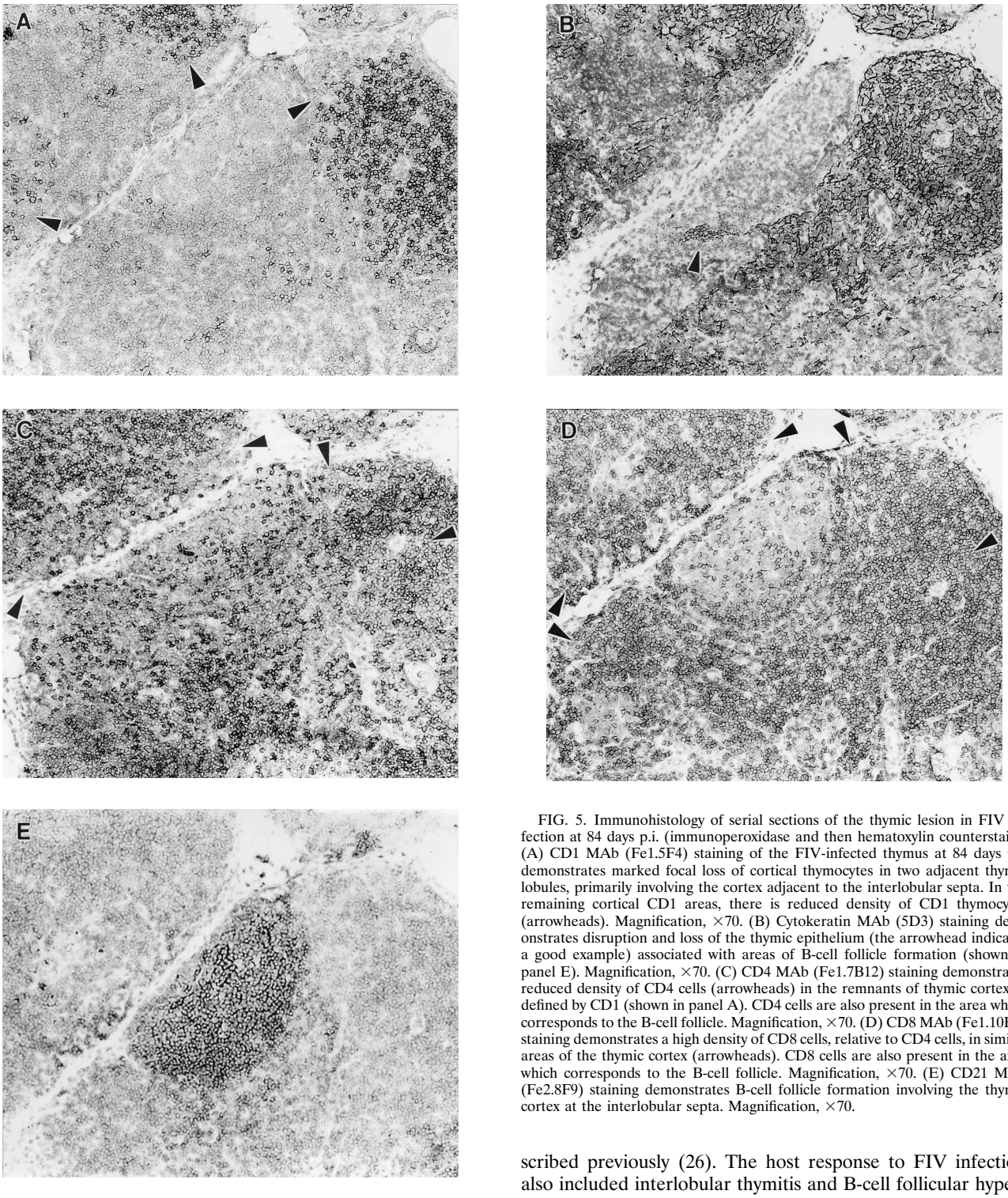

FIG. 5. Immunohistology of serial sections of the thymic lesion in FIV infection at 84 days p.i. (immunoperoxidase and then hematoxylin counterstain). (A) CD1 MAb (Fe1.5F4) staining of the FIV-infected thymus at 84 days p.i. demonstrates marked focal loss of cortical thymocytes in two adjacent thymic lobules, primarily involving the cortex adjacent to the interlobular septa. In the remaining cortical CD1 areas, there is reduced density of CD1 thymocytes (arrowheads). Magnification, ×70. (B) Cytokeratin MAb (5D3) staining demonstrates disruption and loss of the thymic epithelium (the arrowhead indicates a good example) associated with areas of B-cell follicle formation (shown in panel E). Magnification, ×70. (C) CD4 MAb (Fe1.7B12) staining demonstrates reduced density of CD4 cells (arrowheads) in the remnants of thymic cortex as defined by CD1 (shown in panel A). CD4 cells are also present in the area which corresponds to the B-cell follicle. Magnification, ×70. (D) CD8 MAb (Fe1.10E9) staining demonstrates a high density of CD8 cells, relative to CD4 cells, in similar areas of the thymic cortex (arrowheads). CD8 cells are also present in the area which corresponds to the B-cell follicle. Magnification, ×70. (E) CD21 MAb (Fe2.8F9) staining demonstrates B-cell follicle formation involving the thymic cortex at the interlobular septa. Magnification, ×70.

sequent asymptomatic stage of infection. Thymic atrophy, manifested by premature and persistent cortical involution, was evident histologically and quantitatively between 42 and 56 days p.i. and was essentially complete by 96 days p.i. This profound loss of cortical thymocytes in acute FIV infection is similar to findings in naturally occurring neonatal HIV-1 infection, for which thymic involution and selective depletion of $CD4^+$ $CD8^+$ and $CD4^+$ $CD8^-$ thymocytes have been described previously (26). The host response to FIV infection also included interlobular thymitis and B-cell follicular hyperplasia with prominent germinal center formation, which contributed to the distortion of the thymic architecture. This pattern of inflammation and progression of thymic lesions is similar to that previously described for acute retroviral infection in humans with HIV-1 (3), macaques with SIV (15), and mice infected with the murine AIDS virus, RadLV-Rs (5). Although B-cell follicular development has not been quantified in humans or macaques, murine AIDS studies demonstrated marked cortical thymocyte depletion of $CD4^+$ $CD8^+$

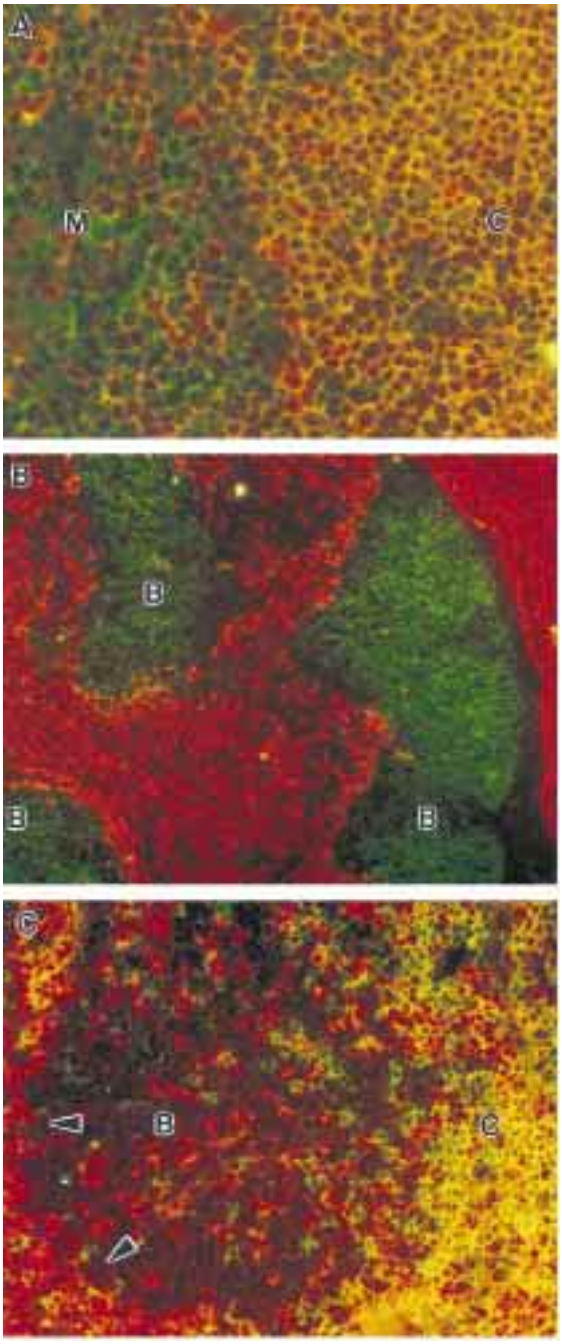

FIG. 6. Double-label immunofluorescent staining of the feline thymus. (A) CD4 MAb (FITC) and CD8 MAb (Texas red) dual staining of the feline thymus in a noninfected control cat at the 70-day time point. The corticomedullary junction is demarcated by the variation in staining. Dual-positive ($CD4^+$ $CD8^+$) cortical thymocytes (C) appear yellow. Single-positive medullary thymocytes (M) appear either green (CD4) or red (CD8). Magnification, ×140. (B) CD22 MAb (FITC) and cytokeratin MAb (Texas red) dual staining of the FIV-infected thymus at 56 days p.i. demonstrates marked lobular architectural distortion due to epithelial disruption and loss (red). Areas of epithelial loss correspond to B-cell domains (B) (green), which extend irregularly through the thymic lobule. Magnification, ×35. (C) CD4 MAb (FITC) and CD8 MAb (Texas red) dual staining of a B-cell area in an FIV-infected thymus at 70 days p.i. The poorly stained area represents a B-cell follicle (B) in the thymic medulla. Dual-positive (CD4-CD8) cortical thymocytes (C) appear yellow. A predominance of single-positive CD8 (red) cells is present within the germinal center and surrounds the B-cell follicle (arrowheads). Fewer single-positive CD4 (green) cells are present in the germinal center. Magnification, ×70.

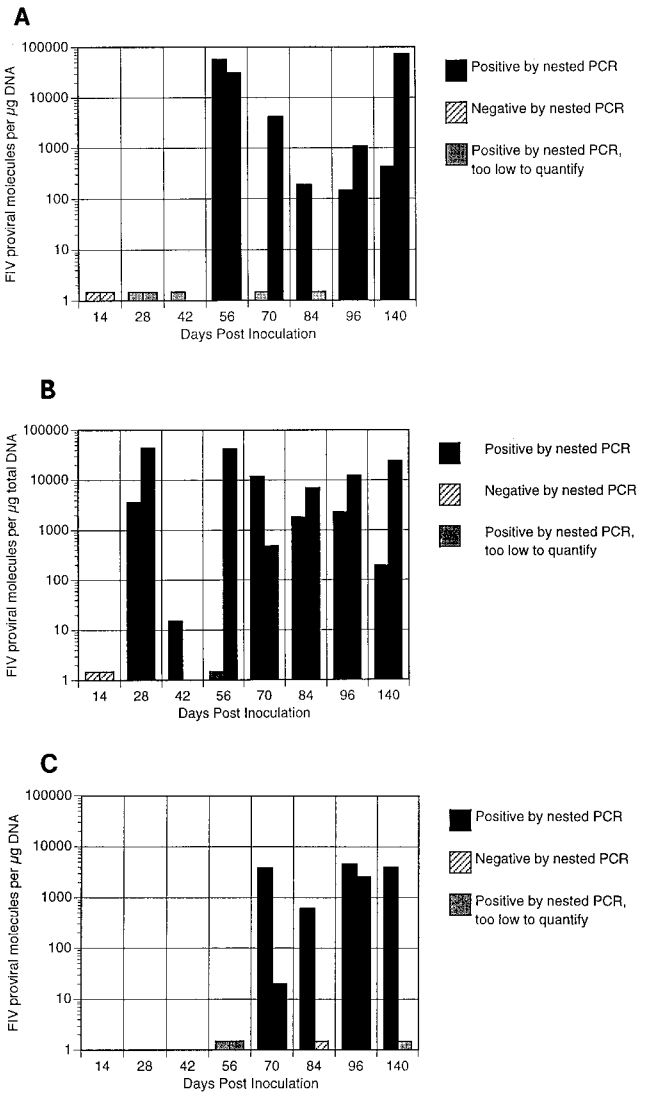

FIG. 7. Quantitated FIV DNA in thymocyte subpopulations in FIV-infected cats at each time point (each bar represents the quantitated viral load in one animal). (A) QC-PCR of $CD1^{hi}$ thymocytes. Low levels of virus within cortical thymocytes were detected as early as 28 days p.i. A marked increase in viral load occurred at 56 days p.i., coinciding with the period of marked inflammation within the thymus. The viral load was maintained at increased levels thereafter throughout the study. (B) QC-PCR of $CD1^{lo}$ thymocytes. Higher levels of provirus were present as early as 28 days p.i. in three cats which exhibited thymitis. The viral load was maintained at increased levels throughout the study. (C) QC-PCR of B cells within the thymus. Viral infection of CD21 and CD22 B cells was detected at low levels at 56 days p.i. but was present at increased levels thereafter.

cells and a progressive increase in B cells (5). The structural changes noted in the present study would suggest that thymic function is compromised.

The effect of FIV infection on thymocyte maturation events was also assessed by examination of CD4 and CD8 expression on $CD1^{hi}$ and $CD1^{lo}$ thymocyte subsets. Adequate numbers of cortical, immature $CD1^{hi}$ thymocytes (with dual expression of CD4 and CD8) were detected prior to 56 days p.i. However, during this period, the mature $CD1^{lo}$ population had decreased numbers of $CD4^+$ $CD8^-$ cells from 28 days p.i. and increased numbers of $CD4^-$ $CD8^+$ cells after 42 days p.i. This would suggest that preferential differentiation of single-posi-

tive CD8 cells, or a preferential cytopathic effect on single-positive CD4 cells, occurred prior to 56 days p.i. However, after 56 days p.i., analysis of T-cell maturation events was confounded by the inflammatory response within the thymus, which was increasingly evident after this time point. After 56 days p.i., the increased number of CD8 cells which lacked CD1 expression, in the face of cortical atrophy, suggests that this marked increase in CD8 cells is primarily associated with infiltrating peripheral T cells rather than maturing medullary thymocytes. The increase in the numbers of CD8 T cells as a component of an inflammatory response was also suggested by immunohistology in which single-positive CD8 cells and few CD4 T cells were associated with B-cell follicles within the thymus.

Assessment of the viral load in the sorted thymocyte subpopulations was also performed to determine specific cellular lymphoid targets in the thymus. The viral DNA burden varied markedly between cortical $CD1^{hi}$ and medullary $CD1^{lo}$ subpopulations prior to 56 days p.i. Cortical thymocytes exhibited low levels of viral infection until 56 days p.i. The dramatic increase in the viral load in this fraction after 56 days coincided with the onset of marked thymic inflammation. This suggests that infiltrating inflammatory cells facilitated infection of immature, cortical $CD1^{hi}$ thymocytes. Contamination of this $CD1^{hi}$ population with $CD1^{lo}$ cells may partly account for the increased proviral burden that was detected. However, the increased proviral burden in this population could not be attributed solely to contaminating cells. Evidence to support viral infection of the $CD1^{hi}$ subpopulation, despite low purity of enrichment, was observed in three cats in which the proviral burden of the $CD1^{hi}$ population was increased in comparison with the proviral burden in the corresponding $CD1^{lo}$ population. By contrast, the increased proviral burden detected in $CD1^{lo}$ fractions from 28 days p.i. and throughout the study suggests that this population was an early and preferential target cell of infection. However, it could not be determined whether the infected $CD1^{lo}$ fraction represented inflammatory cells or mature, medullary thymocytes due to lack of distinguishing feline leukocyte markers. Provirus was also detected, albeit at low levels, in the B-cell fraction at 56 days p.i. The subsequent increase in the B-cell proviral burden, after 70 days p.i., developed during the period in which increasing follicle size and germinal center formation occurred. This suggests that enhanced activation or proliferation of B cells promoted the increased proviral burden. FIV infection of feline B cells has previously been demonstrated in both peripheral blood (8, 11) and mesenteric lymph nodes (8). As in the present study, these studies both describe an increase in the B-cell proviral burden as infection becomes chronic. Provirus was therefore detected in all thymocyte subpopulations. However, the proviral levels detected in the $CD1^{hi}$ population in the present study demonstrated that immature feline thymocytes were permissive for viral infection. This finding is similar to both in vitro (4, 9, 28) and in vivo (4, 6, 27) studies of pediatric HIV-1 infection in humans.

Morphologic alterations, altered thymocyte antigen expression, and productive viral infection suggest that thymic function and therefore thymocyte maturation were severely impaired. As thymic changes were detected from 28 days p.i., the ability of the thymus to replenish the peripheral T-cell pool from this time point is in question. As these changes appear permanent, it is proposed that depletion of the peripheral T-cell pool, which continues throughout the asymptomatic period of infection, can no longer be ameliorated by thymocyte maturation and export of these cells to the peripheral tissues. These conclusions are supported by studies which examine peripheral T-cell depletion in HIV-1 infection by using decreasing telomeric length of peripheral blood T cells as an indication of the replicative history of mature peripheral T-cell subpopulations (21, 29). During the asymptomatic phase of infection, the telomeric length of CD4 T cells was not decreased as expected. It is hypothesized that CD4 T-cell depletion in HIV-1 infection may therefore be associated with failure of T-cell regeneration rather than increased cell turnover (29). However, CD4 T-cell telomeric length decreases in more advanced stages of immunodeficiency (24). Taken together, these studies indicate that the fate and population dynamics of peripheral T cells at different stages of HIV-1 infection have yet to be fully explored.

The morphologic similarities between thymic lesions associated with FIV infection in juvenile cats and those reported for pediatric AIDS patients suggest that FIV is a good model of this aspect of HIV disease. Characterization of events that occur in FIV infection of juvenile cats will enable future studies to examine thymotrophic therapeutic approaches designed to inhibit thymic alterations and promote thymocyte maturation.

ACKNOWLEDGMENTS

We acknowledge Jeff Carlson, Tobie Faith, Joanne Higgins, Alora Lavoy, and Michael Wiseman for their excellent technical assistance; Hong Zhou for assistance with statistical analysis; and Woody Woodward (Miltenyi Biotec) for his generous gift of custom-conjugated CD1 microbeads.

This work was supported by Public Health Service grants AI01262 (to G.A.D.) and AI36189 (to N.C.P.) from NIAID.

REFERENCES

1. **Barlough, J. E., C. D. Ackley, J. W. George, N. Levy, R. Acevedo, P. F. Moore, B. A. Rideout, M. D. Cooper, and N. C. Pedersen.** 1991. Acquired immune dysfunction in cats with experimentally induced feline immunodeficiency virus infection: comparison of short-term and long-term infections. J. Acquired Immune Defic. Syndr. **4:**219–227.
2. **Beebe, A. M., N. Dua, T. G. Faith, P. F. Moore, N. C. Pedersen, and S. Dandekar.** 1994. Primary stage of feline immunodeficiency virus infection: viral dissemination and cellular targets. J. Virol. **68:**3080–3091.
3. **Burke, A. P., D. Anderson, W. Benson, R. Turnicky, P. Mannan, Y. H. Liang, J. Smialek, and R. Virmani.** 1995. Localization of human immunodeficiency virus 1 RNA in thymic tissues from asymptomatic drug addicts. Arch. Pathol. Lab. Med. **119:**36–41.
4. **Calabro, M. L., C. Zanotto, F. Calderazzo, C. Crivellaro, A. Del Mistro, A. De Rossi, and L. Chieco-Bianchi.** 1995. HIV-1 infection of the thymus: evidence for a cytopathic and thymotropic viral variant in vivo. AIDS Res. Hum. Retroviruses **11:**11–19.
5. **Colombi, S., M. Deprez, L. De Leval, C. Humblet, R. Greimers, M. P. Defresne, J. Boniver, and M. Moutschen.** 1994. Thymus involvement in murine acquired immunodeficiency (MAIDS). Thymus **23:**27–37.
6. **Courgnaud, V., F. Laure, A. Brossard, C. Bignozzi, A. Goudeau, F. Barin, and C. Brechot.** 1991. Frequent and early in utero HIV-1 infection. AIDS Res. Hum. Retroviruses **7:**337–341.
7. **Dandekar, S., A. M. Beebe, J. Barlough, T. Phillips, J. Elder, M. Torten, and N. Pedersen.** 1992. Detection of feline immunodeficiency virus (FIV) nucleic acids in FIV-seronegative cats. J. Virol. **66:**4040–4049.
8. **Dean, G. A., G. H. Reubel, P. F. Moore, and N. C. Pedersen.** 1996. Proviral burden and infection kinetics of feline immunodeficiency virus in lymphocyte subsets of blood and lymph node. J. Virol. **70:**5165–5169.
9. **De Rossi, A., M. L. Calabro, M. Panozzo, D. Bernardi, B. Caruso, G. Tridente, and L. Chieco-Bianchi.** 1990. In vitro studies of HIV-1 infection in thymic lymphocytes: a putative role of the thymus in AIDS pathogenesis. AIDS Res. Hum. Retroviruses **6:**287–298.
10. **Dua, N., G. Reubel, P. F. Moore, J. Higgins, and N. C. Pedersen.** 1994. An experimental study of primary feline immunodeficiency virus infection in cats and a historical comparison to acute simian and human immunodeficiency virus diseases. Vet. Immunol. Immunopathol. **43:**337–355.
11. **English, R. V., P. Nelson, C. M. Johnson, M. Nasisse, W. A. Tompkins, and M. B. Tompkins.** 1994. Development of clinical disease in cats experimentally infected with feline immunodeficiency virus. J. Infect. Dis. **170:**543–552.
12. **Frederick, T., L. Mascola, A. Eller, L. O'Neil, and B. Byers.** 1994. Progression of human immunodeficiency virus disease among infants and children infected perinatally with human immunodeficiency virus or through neonatal

blood transfusion. Los Angeles County Pediatric AIDS Consortium and the Los Angeles County-University of Southern California Medical Center and the University of Southern California School of Medicine. Pediatr. Infect. Dis. J. **13:**1091–1097.
13. **Kneitz, C., T. Kerkau, J. Muller, C. Coulibaly, C. Stahl-Hennig, G. Hunsmann, T. Hunig, and A. Schimpl.** 1993. Early phenotypic and functional alterations in lymphocytes from simian immunodeficiency virus infected macaques. Vet. Immunol. Immunopathol. **36:**239–255.
14. **Lackner, A. A., P. Vogel, R. A. Ramos, J. D. Kluge, and M. Marthas.** 1994. Early events in tissues during infection with pathogenic (SIVmac239) and nonpathogenic (SIVmac1A11) molecular clones of simian immunodeficiency virus. Am. J. Pathol. **145:**428–439.
15. **Li, S. L., E. E. Kaaya, C. Ordonez, M. Ekman, H. Feichtinger, P. Putkonen, D. Bottiger, G. Biberfeld, and P. Biberfeld.** 1995. Thymic immunopathology and progression of SIVsm infection in cynomolgus monkeys. J. Acquired Immune Defic. Syndr. Hum. Retrovirol. **9:**1–10.
16. **McKinney, R. E., Jr., and C. M. Wilfert.** 1992. Lymphocyte subsets in children younger than 2 years old: normal values in a population at risk for human immunodeficiency virus infection and diagnostic and prognostic application to infected children. Pediatr. Infect. Dis. J. **11:**639–644.
17. **Moore, P. F., P. V. Rossitto, D. M. Danilenko, J. J. Wielenga, R. F. Raff, and E. Severns.** 1992. Monoclonal antibodies specific for canine CD4 and CD8 define functional T-lymphocyte subsets and high-density expression of CD4 by canine neutrophils. Tissue Antigens **40:**75–85.
18. **Muller, J. G., S. Czub, A. Marx, R. Brinkmann, R. Plesker, and H. K. Muller-Hermelink.** 1994. Detection of SIV in rhesus monkey thymus stroma cell cultures. Res. Virol. **145:**239–244.
19. **Muller, J. G., V. Krenn, S. Czub, C. Stahl-Hennig, C. Coulibaly, G. Hunsmann, and H. K. Muller-Hermelink.** 1993. The thymic epithelial reticulum and interdigitating cells in SIV-induced thymus atrophy and its comparison with other forms of thymus involution. Res. Virol. **144:**93–98.
20. **Muller, J. G., V. Krenn, C. Schindler, S. Czub, C. Stahl-Hennig, C. Coulibaly, G. Hunsmann, C. Kneitz, T. Kerkau, A. Rethwilm, V. terMeulen, and H. K. Muller-Hermelink.** 1993. Alterations of thymus cortical epithelium and interdigitating dendritic cells but no increase of thymocyte cell death in the early course of simian immunodeficiency virus infection. Am. J. Pathol. **143:**699–713.
21. **Palmer, L. D., N. Weng, B. I. Levine, C. H. June, H. C. Lane, and R. J. Hodes.** 1997. Telomere length, telomerase activity, and replicative potential in HIV infection: analysis of $CD4^-$ and $CD8^+$ T cells from HIV-discordant monozygotic twins. J. Exp. Med. **185:**1381–1386.
22. **Papiernik, M., Y. Brossard, N. Mulliez, J. Roume, C. Brechot, F. Barin, A. Goudeau, J. F. Bach, C. Griscelli, and R. Henrion.** 1992. Thymic abnormalities in fetuses aborted from human immunodeficiency virus type 1 seropositive women. Pediatrics **89:**297–301.
23. **Phillips, T. R., R. L. Talbott, C. Lamont, S. Muir, K. Lovelace, and J. H. Elder.** 1990. Comparison of two host cell range variants of feline immunodeficiency virus. J. Virol. **64:**4605–4613.
24. **Pommier, J.-P., L. Gauthier, J. Livartowski, P. Galanaud, F. Boue, A. Duliost, D. Marce, C. Ducray, L. Sabatier, J. Lebeau, and F.-D. Boussin.** 1997. Immunosenescence in HIV pathogenesis. Virology **231:**148–153.
25. **Reubel, G. H., J. W. George, J. Higgins, and N. C. Pedersen.** 1994. Effect of chronic feline immunodeficiency virus infection on experimental feline calicivirus-induced disease. Vet. Microbiol. **39:**335–351.
26. **Rosenzweig, M., D. P. Clark, and G. N. Gaulton.** 1993. Selective thymocyte depletion in neonatal HIV-1 thymic infection. AIDS **7:**1601–1605.
27. **Schnittman, S. M., S. M. Denning, J. J. Greenhouse, J. S. Justement, M. Baseler, J. Kurtzberg, B. F. Haynes, and A. S. Fauci.** 1990. Evidence for susceptibility of intrathymic T-cell precursors and their progeny carrying T-cell antigen receptor phenotypes TCR alpha beta+ and TCR gamma delta+ to human immunodeficiency virus infection: a mechanism for CD4+ (T4) lymphocyte depletion. Proc. Natl. Acad. Sci. USA **87:**7727–7731.
28. **Valentin, H., M. T. Nugeyre, F. Vuillier, L. Boumsell, M. Schmid, F. Barre-Sinoussi, and R. A. Pereira.** 1994. Two subpopulations of human triple-negative thymic cells are susceptible to infection by human immunodeficiency virus type 1 in vitro. J. Virol. **68:**3041–3050.
29. **Wolthers, C. K., G. B. A. Wisman, S. A. Otto, A.-M. de Roda Husman, N. Schaft, F. de Wolf, J. Goudsmit, R. A. Coutinho, A. G. J. van der Zee, L. Meyaard, and F. Miedema.** 1996. T cell telomere length in HIV-1 infection: no evidence for increased CD4+ T cell turnover. Science **274:**1543–1547.
30. **Woo, J. C., and P. F. Moore.** 1997. A feline homologue of CD1 is defined using a feline-specific monoclonal antibody. Tissue Antigens **49:**244–251.
31. **Zachar, V., R. A. Thomas, and A. S. Goustin.** 1993. Absolute quantification of target DNA: a simple competitive PCR for efficient analysis of multiple samples. Nucleic Acids Res. **21:**2017–2018.